THE ASTROPHYSICAL JOURNAL, 305:136–147, 1986 June 1


# DYNAMICS OF THE ELLIPTICAL GALAXY NGC 7097 MEASURED FROM GAS AND STARS

NELSON CALDWELL
Cerro Tololo Inter-American Observatory, National Optical Astronomy Observatories
AND
ROBERT P. KIRSHNER[1] AND DOUGLAS O. RICHSTONE
Department of Astronomy, University of Michigan
*Received 1985 April 15; accepted 1985 November 25*

## ABSTRACT

The E4 galaxy NGC 7097 is normal on broad-band photographs and has the surface-brightness profile of an ordinary elliptical galaxy. Spectra taken at the CTIO 4 m show that NGC 7097 has extended [O II] and [O III] emission which provides an unusual opportunity to use the motion of the gas to probe the radial mass distribution of an elliptical galaxy. Our observations are consistent with a centrally concentrated gas disk of radius 15″ (4 kpc) inclined at 60° to the plane of the sky. If the gas velocities are circular, they can be used to determine $M(r)$ for this galaxy. The inferred mass distribution of the galaxy has a larger scale length than the scale length of the stellar distribution, so that the mass-to-light ratio increases from below 1 at the center to 3.5 at 3 kpc. In the absence of a variation in the stellar composition, this is evidence for dark matter in an elliptical galaxy.

Analysis of stellar rotation and velocity dispersion distributions through linear programming methods shows that to match the observed mass and light distributions, the radial component of the stellar velocity dispersions must be larger than the tangential dispersions.

*Subject headings:* galaxies: individual — galaxies: internal motions

## I. INTRODUCTION

A survey by Caldwell (1984) of the frequency of ionized gas in elliptical galaxies revealed strong and spatially extended [O II] emission in the E4 galaxy NGC 7097. While in general the mass distribution in elliptical galaxies has proved very difficult to determine from stellar velocities and velocity dispersions, the presence of an ionized gas disk in this galaxy provides the rare opportunity to determine the mass distribution in a normal elliptical galaxy. As Figure 1 shows and surface photometry presented in § II details, the galaxy appears normal, with no morphological peculiarities.

To measure the rotation of the ionized gas, as well as the rotation and velocity dispersion of the stars, we obtained image-tube spectra at four position angles with the Ritchey-Chrétien (RC) spectrograph at the CTIO 4 m telescope. As described in § II, the spectra were of sufficient quality to provide dynamical information up to 15″ (4 kpc) from the galaxy center (we adopt a distance to NGC 7097 of 52 Mpc, corresponding to $H = 50$ km s$^{-1}$ Mpc$^{-1}$).

The observed rotation curves and the distribution of emission are consistent with a gas disk inclined to the line of sight. If the gas is in circular orbits, we can derive the mass distribution of the galaxy. As shown in § III, the resulting blue mass-to-light ratio of the galaxy is not constant, ranging from below 1 near the center to 3.5 at 12″. In the absence of a change in the stellar population, this result points to the presence of dark matter in this elliptical galaxy that has a scale length larger than that of the stars.

In § IV, we use the light distribution, the stellar velocity distribution, and the mass distribution derived from the gas velocities to construct models for the stellar orbits using linear programming methods. These models have dispersion tensors which are anisotropic with larger radial than tangential dispersions in the inner region of this galaxy. Isotropic stellar velocity distributions are excluded by the observations. The dominance of radial orbits is a fundamental property of this galaxy which may provide hints about the process of galaxy formation.

## II. OBSERVATIONS AND ANALYSIS

The spectroscopic material consists of four baked IIIa-J plates taken with the RC spectrograph and Carnegie image tube on the CTIO 4 m telescope. A 632 line mm$^{-1}$ grating blazed at 4200 Å was employed, which, when used with a 1″.5 slit, gave a resolution of ~3.5 Å. The plate scale was 25″.4 mm$^{-1}$. All of the spectra were taken with the slit passing through the galaxy center, but oriented at different position angles. The major and minor axes of the galaxy image were observed (position angles 18°.5 and 108°.5, respectively), as were two skewed angles (38°.5 and 153°.5). The plates were digitized with a PDS microdensitometer at a pixel size corresponding to 0.4 Å by 1″.0, and the densities were converted to intensities via calibration spots. Wavelength corrections were determined by fitting a fifth-order polynomial to the comparison spectra above and below the galaxy spectra. These corrections were then applied to both the galaxy spectra and the full-slit comparison line exposure recorded on each plate. The curvatures of the comparison lines along the slit on the full-slit exposure were fitted with a third-order polynomial, and these wavelength corrections were also applied to the galaxy spectra to remove slit curvature. When these corrections were applied to the full-slit comparison exposures, no single corrected comparison line showed a curvature greater than 0.5 km s$^{-1}$ per arcsecond along the slit, and the average remaining curvature

[1] Visiting Astronomer, Cerro Tololo Inter-American Observatory, National Optical Astronomy Observatories, operated by AURA, Inc., under contract with the National Science Foundation.

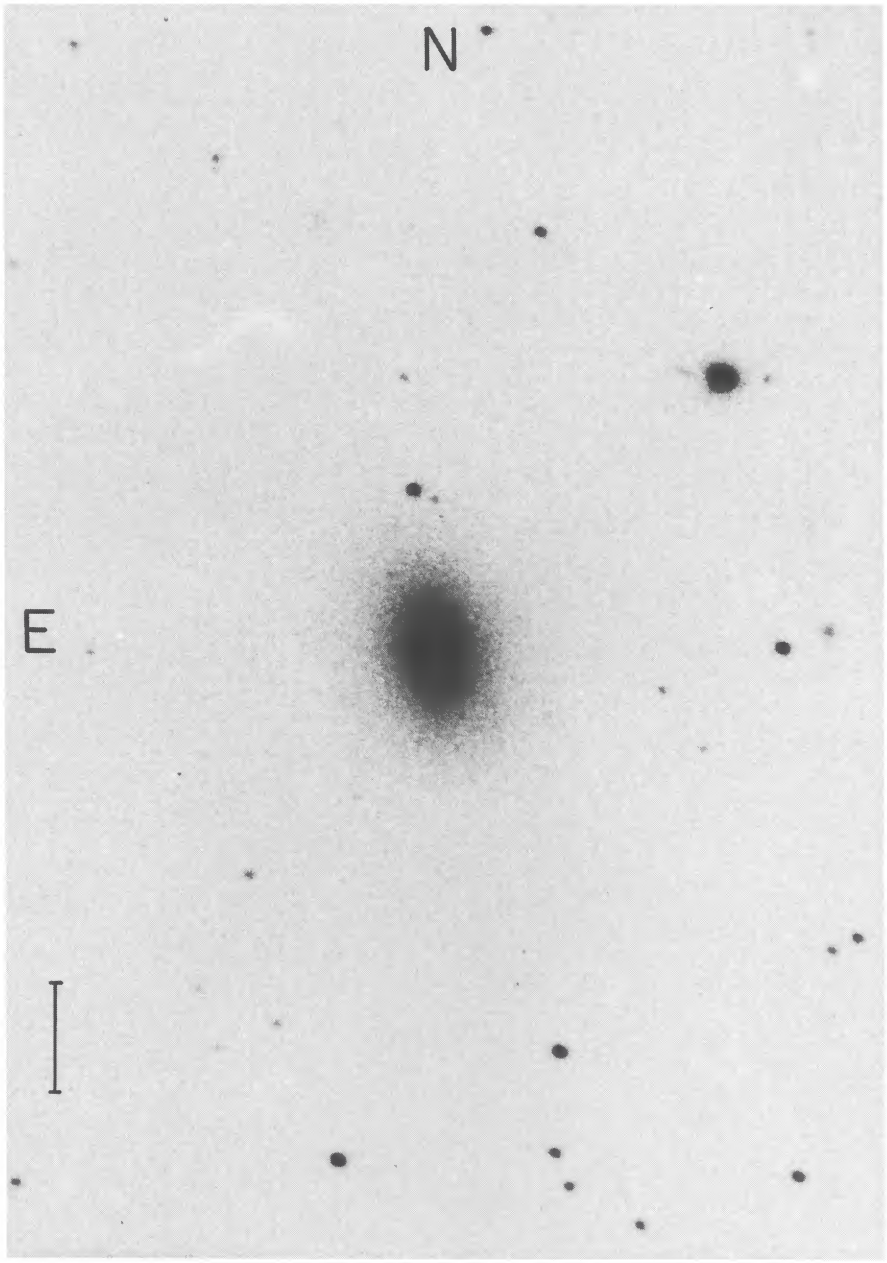


FIG. 1.—*B*-band image-tube photograph of NGC 7097 obtained at CTIO with the Yale 1 m telescope

among the lines was negligible. The spatial distortions in the galaxy spectra were mapped by fitting a cubic polynomial to the slit positions of maximum intensity at each wavelength position. The galaxy spectra were then shifted in the spatial direction as dictated by this polynomial to create a rectified spectrum.

The gas velocities were obtained by measuring the centroid of the [O II] and [O III] lines, assuming an effective wavelength of $\lambda 3727.3$ for the [O II] doublet. While it is conceivable that density changes could change the effective wavelength of this doublet and mimic velocity changes, we believe this is unlikely. The work of Demoulin-Ulrich, Butcher, and Boksenberg (1984) and Bertola *et al.* (1984) show that for other elliptical galaxies, the density of the ionized gas changes so slowly as to have a negligible effect on the effective wavelength of the [O II] doublet. In the worst (and most unlikely) case the velocity difference caused by changes in the gas density would be 50 km $s^{-1}$, yet we see velocities of 200 km $s^{-1}$.

A spectrum of a K0 III star served as a template to determine the stellar velocities and dispersions via the Fourier quotient technique (Sargent *et al.* 1978). The H and K lines and the *G*-band spectral region were excluded from the dispersion fits. In general, the stellar velocities have an accuracy of $\sim 10$ km $s^{-1}$ where the spectra are well exposed, and the velocity dispersions have internal errors of $\sim 15$ km $s^{-1}$.

The velocities of stars and gas and the stellar dispersions together with their errors are listed in Table 1 and are displayed in Figures 2–5. The systemic velocity of $2601 \pm 10$ km $s^{-1}$ has been subtracted from stellar and gas velocities. On the major axis (Fig. 2) the gas velocities rise rapidly, leveling off near 200 km $s^{-1}$. The north side of the gas distribution is receding. The emission is detected to $\sim 15''$ in radius. The stellar rotation is very slow, but probably not zero. On the north side, the stars are approaching. That is, the stars and gas are rotating in opposite directions, and they have very different velocities. The stellar velocity dispersions are near 250 km $s^{-1}$ near the center, falling to 100–150 km $s^{-1}$ at $R = 20''$.

On the minor axis (Fig. 3) the gas velocities are very small: any velocity on the minor axis must be smaller than 30 km $s^{-1}$. The emission only extends to $7''$ from the center along the minor axis. The stellar velocities on the minor axis are also small. The stellar velocity dispersion is near 180 km $s^{-1}$ at the galaxy center, declining to 100–150 km $s^{-1}$ at $R = 10''$. The difference in central dispersion measurements

TABLE 1

KINEMATIC DATA ON NGC 7097

A.

| PLATE 2185, $\phi = 38.5$ GAS | | | PLATE 2179, $\phi = 18.5$ GAS | | | PLATE 2185, $\phi = 38.5$ STARS | | | PLATE 2179, $\phi = 18.5$ STARS | | |
|---|---|---|---|---|---|---|---|---|---|---|---|
| $r$ | Line | Velocity | $r$ | Line | Velocity | $r$ | Velocity | $\sigma$ | $r$ | Velocity | $\sigma$ |
| −12.6... | 3727 | −210 | −13.8... | 3727 | −217 | −23.9... | 31 ± 32 | ... | −19.7... | 51 ± 23 | 104 ± 34 |
| −11.6... | 3727 | −217 | −12.8... | 3727 | −165 | −19.9... | 39 ± 20 | 152 ± 30 | −16.7... | 12 ± 17 | 138 ± 25 |
| −9.7... | 3727 | −208 | −11.8... | 3727 | −106 | −16.5... | 40 ± 17 | 160 ± 28 | −14.3... | 35 ± 15 | 141 ± 20 |
| −8.7... | 3727 | −225 | −10.9... | 3727 | −158 | −13.6... | 6 ± 13 | 108 ± 19 | −12.3... | 38 ± 15 | 172 ± 17 |
| −7.7... | 3727 | −188 | −9.9... | 3727 | −184 | −11.1... | −15 ± 15 | 175 ± 21 | −10.4... | 15 ± 13 | 191 ± 18 |
| −6.7... | 3727 | −165 | −8.9... | 3727 | −137 | −9.2... | 23 ± 14 | 206 ± 18 | −8.9... | 4 ± 12 | 199 ± 17 |
| −5.7... | 3727 | −167 | −7.9... | 3727 | −141 | −7.2... | 19 ± 10 | 195 ± 14 | −7.9... | 28 ± 12 | 202 ± 16 |
| −4.8... | 3727 | −174 | −6.9... | 3727 | −154 | −5.7... | 25 ± 11 | 231 ± 16 | −6.9... | 21 ± 12 | 218 ± 18 |
| −3.8... | 3727 | −167 | −6.0... | 3727 | −156 | −4.8... | 39 ± 10 | 219 ± 15 | −6.0... | 25 ± 11 | 229 ± 16 |
| −2.8... | 3727 | −133 | −5.0... | 3727 | −170 | −3.8... | 26 ± 10 | 198 ± 13 | −5.0... | 35 ± 10 | 236 ± 14 |
| −1.8... | 3727 | −97 | −4.0... | 3727 | −142 | −2.8... | 15 ± 11 | 225 ± 18 | −4.0... | 36 ± 12 | 241 ± 16 |
| −0.8... | 3727 | −37 | −4.0... | 5007 | −163 | −1.8... | 12 ± 12 | 192 ± 21 | −3.0... | 14 ± 11 | 242 ± 16 |
| 0.1... | 3727 | −34 | −3.0 | 3727 | −115 | −0.8... | 11 ± 20 | 191 ± 37 | −2.0... | 4 ± 12 | 238 ± 17 |
| 1.1... | 3727 | −24 | −3.0... | 5007 | −187 | 0.1... | −7 ± 25 | 161 ± 38 | −1.1... | −6 ± 13 | 241 ± 20 |
| 2.1... | 3727 | 7 | −2.0... | 3727 | −64 | 1.1... | −19 ± 14 | 150 ± 25 | −0.1... | −2 ± 13 | 221 ± 22 |
| 3.1... | 3727 | 32 | −1.1... | 3727 | −11 | 2.1... | −19 ± 10 | 155 ± 16 | 0.9... | −13 ± 14 | 204 ± 22 |
| 4.1... | 3727 | 41 | −1.1... | 5007 | −87 | 3.1... | −18 ± 10 | 209 ± 15 | 1.9... | −12 ± 13 | 266 ± 22 |
| 5.0... | 3727 | 41 | −0.1... | 3727 | 17 | 4.1... | 0 ± 10 | 194 ± 14 | 2.9... | −26 ± 12 | 260 ± 18 |
| 6.0... | 3727 | 92 | 0.9... | 3727 | 28 | 5.0... | −2 ± 10 | 200 ± 15 | 3.8... | −25 ± 11 | 247 ± 17 |
| 7.0... | 3727 | 113 | 0.9... | 5007 | 84 | 6.0... | −26 ± 10 | 213 ± 15 | 4.8... | −2 ± 11 | 221 ± 15 |
| 8.0... | 3727 | 138 | 1.9... | 3727 | 51 | 7.0... | 0 ± 11 | 187 ± 16 | 5.8... | −7 ± 10 | 224 ± 15 |
| 9.0... | 3727 | 225 | 1.9... | 5007 | 57 | 8.0... | −8 ± 12 | 216 ± 18 | 6.8... | 4 ± 12 | 230 ± 17 |
| | | | 2.9... | 3727 | 94 | 9.0... | −3 ± 10 | 186 ± 18 | 7.8... | 12 ± 13 | 213 ± 18 |
| | | | 3.8... | 3727 | 128 | 9.9... | −21 ± 11 | 177 ± 18 | 8.7... | 17 ± 12 | 195 ± 19 |
| | | | 3.8... | 5007 | 139 | 10.9... | −10 ± 14 | 193 ± 19 | 9.7... | −4 ± 14 | 184 ± 23 |
| | | | 4.8... | 3727 | 144 | 11.9... | −5 ± 15 | 180 ± 18 | 11.2... | 0 ± 14 | 185 ± 19 |
| | | | 4.8... | 5007 | 170 | 12.9... | 37 ± 15 | 174 ± 19 | 13.2... | 2 ± 15 | 218 ± 22 |
| | | | 5.8... | 3727 | 182 | 13.9... | 52 ± 14 | 126 ± 29 | 15.1... | 37 ± 16 | 209 ± 21 |
| | | | 5.8... | 5007 | 204 | 14.8... | 66 ± 19 | 117 ± 37 | 17.6... | 22 ± 22 | 167 ± 27 |
| | | | 6.8... | 3727 | 196 | 16.3... | 13 ± 25 | ... | 20.5... | 24 ± 27 | 149 ± 31 |
| | | | 7.8... | 3727 | 206 | 18.3... | 84 ± 17 | 118 ± 28 | 23.9... | 14 ± 20 | 116 ± 28 |
| | | | 8.7... | 3727 | 212 | | | | | | |
| | | | 9.7... | 3727 | 246 | | | | | | |
| | | | 10.7... | 3727 | 277 | | | | | | |
| | | | 11.7... | 3727 | 181 | | | | | | |
| | | | 12.7... | 3727 | 199 | | | | | | |
| | | | 13.6... | 3727 | 155 | | | | | | |
| | | | 14.6... | 3727 | 128 | | | | | | |

TABLE 1—*Continued*

B.

| PLATE 2180, $\phi = 108.5$ GAS | | | PLATE 2186, $\phi = 153.5$ GAS | | | PLATE 2180, $\phi = 108.5$ STARS | | | PLATE 2186, $\phi = 153.5$ STARS | | |
|---|---|---|---|---|---|---|---|---|---|---|---|
| $r$ | Line | Velocity | $r$ | Line | Velocity | $r$ | Velocity | $\sigma$ | $r$ | Velocity | $\sigma$ |
| −7.2... | 3727 | 21 | −9.3... | 3727 | 166 | −11.6... | −5 ± 31 | 137 ± 40 | −16.2... | 32 ± 22 | 124 ± 29 |
| −6.2... | 3727 | 58 | −8.3... | 3727 | 142 | −10.1... | 20 ± 29 | 192 ± 32 | −13.7... | 11 ± 16 | 121 ± 23 |
| −5.2... | 3727 | −6 | −7.4... | 3727 | 98 | −9.1... | 51 ± 22 | 187 ± 27 | −11.8... | 28 ± 12 | 145 ± 18 |
| −5.2... | 5007 | 14 | −6.4... | 3727 | 115 | −8.2... | 37 ± 19 | 178 ± 26 | −9.8... | −4 ± 12 | 164 ± 18 |
| −4.2... | 3727 | −18 | −5.4... | 3727 | 128 | −7.2... | 42 ± 18 | 143 ± 25 | −8.3... | 16 ± 13 | 187 ± 18 |
| −4.2... | 5007 | 21 | −5.4... | 5007 | 66 | −6.2... | 22 ± 19 | 213 ± 24 | −7.4... | 37 ± 10 | 164 ± 15 |
| −3.3... | 3727 | 22 | −4.4... | 3727 | 149 | −5.2... | 31 ± 12 | 166 ± 16 | −6.4... | 23 ± 8 | 174 ± 14 |
| −2.3... | 3727 | 22 | −4.4... | 5007 | 111 | −4.2... | 28 ± 10 | 170 ± 16 | −5.4... | 14 ± 9 | 176 ± 15 |
| −1.3... | 3727 | 3 | −3.4... | 3727 | 146 | −3.3... | 10 ± 10 | 182 ± 14 | −4.4... | 5 ± 10 | 183 ± 17 |
| −0.3... | 3727 | −3 | −2.5... | 5007 | 77 | −2.3... | 12 ± 9 | 193 ± 14 | −3.4... | 10 ± 9 | 194 ± 14 |
| 0.7... | 3727 | 4 | −1.5... | 3727 | 119 | −1.3... | 1 ± 11 | 189 ± 17 | −2.5... | −4 ± 9 | 182 ± 14 |
| 1.6... | 3727 | 1 | −1.5... | 5007 | 27 | −0.3... | 13 ± 12 | 163 ± 20 | −1.5... | −27 ± 11 | 188 ± 16 |
| 2.6... | 3727 | −17 | −0.5... | 3727 | 82 | 0.7... | −10 ± 12 | 225 ± 20 | −0.5... | −25 ± 12 | 164 ± 19 |
| 3.6... | 3727 | −43 | −0.6... | 5007 | 13 | 1.6... | −19 ± 12 | 201 ± 20 | 0.5... | −5 ± 13 | 169 ± 19 |
| 4.6... | 3727 | −37 | 0.5... | 3727 | 43 | 2.6... | −29 ± 12 | 223 ± 19 | 1.5... | 4 ± 11 | 175 ± 20 |
| 5.6... | 3727 | −15 | 0.5... | 5007 | −1 | 3.6... | −10 ± 10 | 189 ± 16 | 2.4... | 20 ± 9 | 174 ± 15 |
| 6.5... | 3727 | 19 | 1.5... | 3727 | 5 | 4.6... | −4 ± 11 | 185 ± 17 | 3.4... | 22 ± 8 | 195 ± 15 |
| 8.5... | 3727 | −14 | 1.5... | 5007 | −64 | 5.6... | −6 ± 12 | 191 ± 19 | 4.4... | 46 ± 8 | 177 ± 13 |
| | | | 2.4... | 3727 | −52 | 6.5... | 17 ± 14 | 177 ± 20 | 5.4... | 45 ± 8 | 181 ± 13 |
| | | | 2.4... | 5007 | −91 | 8.0... | 32 ± 12 | 118 ± 19 | 6.4... | 43 ± 10 | 202 ± 16 |
| | | | 3.4... | 3727 | −94 | | | | 7.3... | 37 ± 11 | 191 ± 16 |
| | | | 3.4... | 5007 | −102 | | | | 8.3... | 33 ± 15 | 162 ± 18 |
| | | | 4.4... | 3727 | −111 | | | | 9.3... | 44 ± 12 | 104 ± 16 |
| | | | 4.4... | 5007 | −80 | | | | 10.3... | 66 ± 14 | 133 ± 20 |
| | | | 5.4... | 3727 | −67 | | | | 11.7... | 39 ± 14 | 123 ± 22 |
| | | | 5.4... | 5007 | −66 | | | | 13.7... | 51 ± 17 | 110 ± 24 |
| | | | 6.5... | 3727 | −77 | | | | 15.7... | 23 ± 20 | ... |
| | | | 7.3... | 3727 | −24 | | | | | | |
| | | | 7.3... | 5007 | −110 | | | | | | |
| | | | 8.3... | 3727 | −24 | | | | | | |
| | | | 9.3... | 3727 | −2 | | | | | | |
| | | | 9.3... | 5007 | −118 | | | | | | |
| | | | 10.3... | 3727 | −55 | | | | | | |
| | | | 11.3... | 3727 | −79 | | | | | | |
| | | | 12.2... | 3727 | −100 | | | | | | |
| | | | 13.2... | 3727 | −16 | | | | | | |

between the minor and major axes is resolved by examining the other two spectra (Figs. 4 and 5) which confirm a central velocity dispersion near 200 km $s^{-1}$. Although the amplitude of the stellar rotation is small, all the spectra are consistent with the gas in a disk aligned with the major axis of the galaxy, but counterrotating with respect to the stars.

The distribution of both the emission-line gas and the starlight has also been measured, and is used in the analysis of § III. In particular, the $\lambda$3727 line emission as observed on our spectrograms is roughly symmetric about the galaxy center and extends ~15″ along the major axis.

To analyze the stellar light distribution, we photographed NGC 7097 with the image-tube camera on the 1 m telescope at CTIO. This IIIa-J plate, exposed with a blue filter, and a plate containing calibration spots were scanned with a PDS. After converting densities to intensities and subtracting the sky background obtained from the edges of the field, we set the photometric zero point by comparing a simulated aperture measurement with the photoelectric photometry of Sandage and Visvanathan (1978). Isophotal contours were then located by an ellipse fitting program. The surface brightness distribution with respect to the harmonic radius of the ellipse is given in Figure 6. The best-fitting $R^{1/4}$ law (which has an effective radius of 4.86 kpc) is shown as a line through the data: the good quality of the fit confirms the impression from Figure 1 that we are indeed dealing with a normal elliptical galaxy. The seeing in this image was ~1″.5. Additional CCD photometry obtained in poor seeing confirms the photometric accuracy of this surface brightness distribution, but adds no useful information on the inner regions of NGC 7097.

## III. INTERPRETING THE GAS DYNAMICAL DATA

The extent and velocity of the gas distribution are known at eight position angles from the four spectra. In this section we show that an adequate model for the observations is that the galaxy has an inclined disk of gas in circular orbits. While such a model is not unique, it is simple and accounts for all the observations. The strength of the emission lines as a function of distance from the center suggests that the disk is filled.

For gas in a thin disk at an inclination $i$, we assume a radial distribution of emissivity $\epsilon(r)$. If $\epsilon(r)$ has a sharp edge at some $r$, the disk inclination can be determined from the maximum gas extent along the major ($x$) axis and the minor ($y$) axis since $y$ max/$x$ max = cos $i$. Examination of Figures 2 and 3 shows $i$ is near 60°. The extent in any direction $\phi$ (on the sky) relative to the major axis $\phi_0$ is easily shown to be

$$r/x_{\max} = [1 + \tan^2 i \sin^2 (\phi - \phi_0)]^{-1/2} . \quad (1)$$

This equation also agrees with the gas extent in the other directions illustrated in Figures 4 and 5, so we adopt $i = 60°$

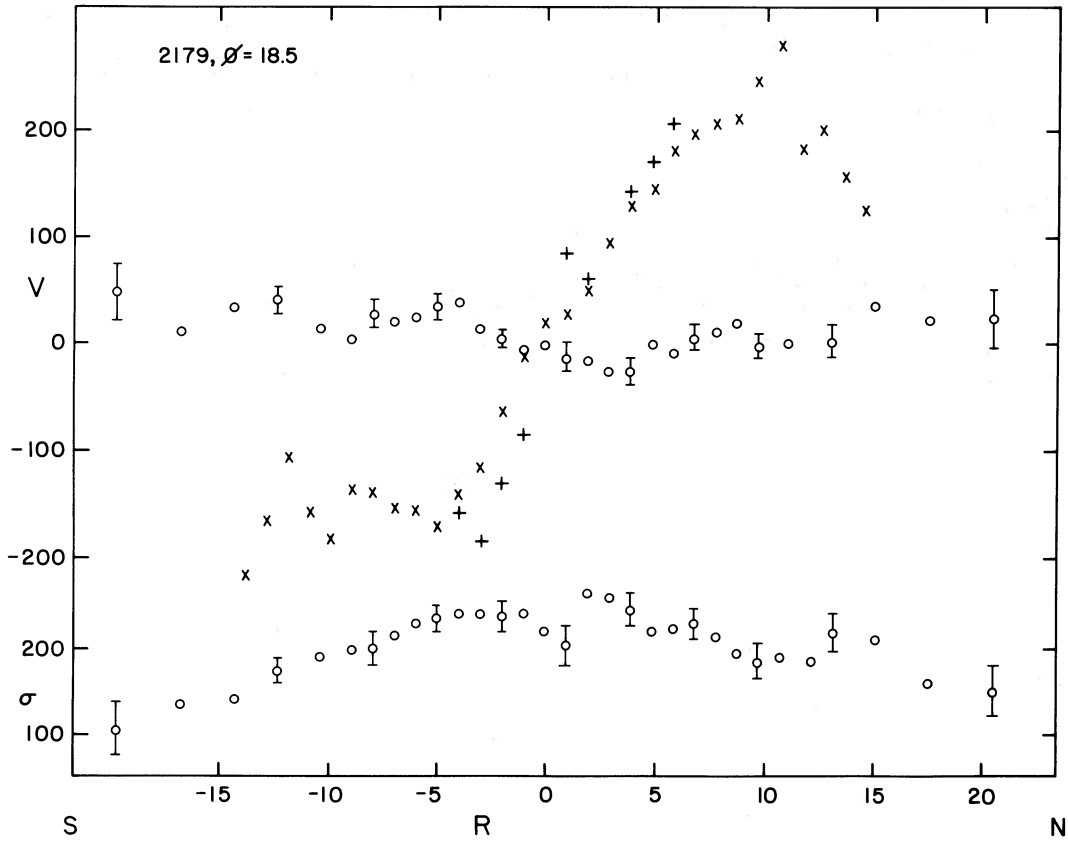


FIG. 2.—Major axis rotation curve (P.A. = 18.5) for [O II] (*cross*), [O III] (*plus*), and stars (*open circle*) and the stellar velocity dispersion profile for NGC 7097

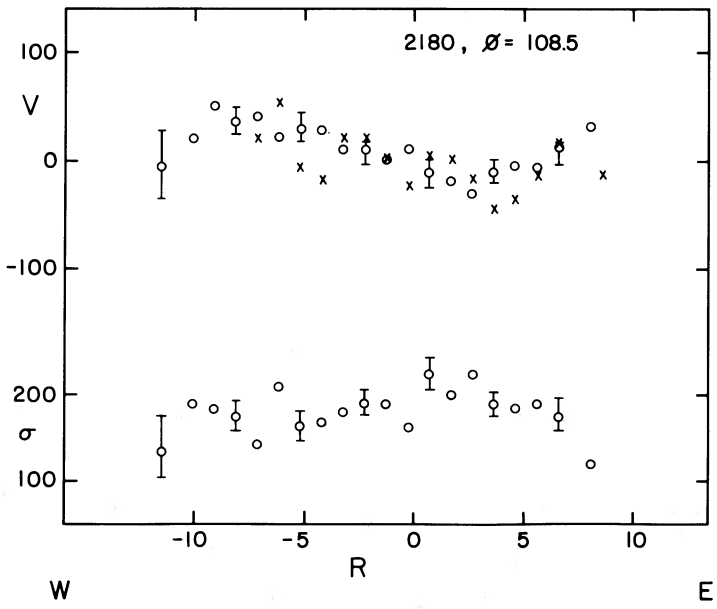


FIG. 3.—Minor axis rotation curve and velocity dispersion profile. Symbols as in Fig. 2.

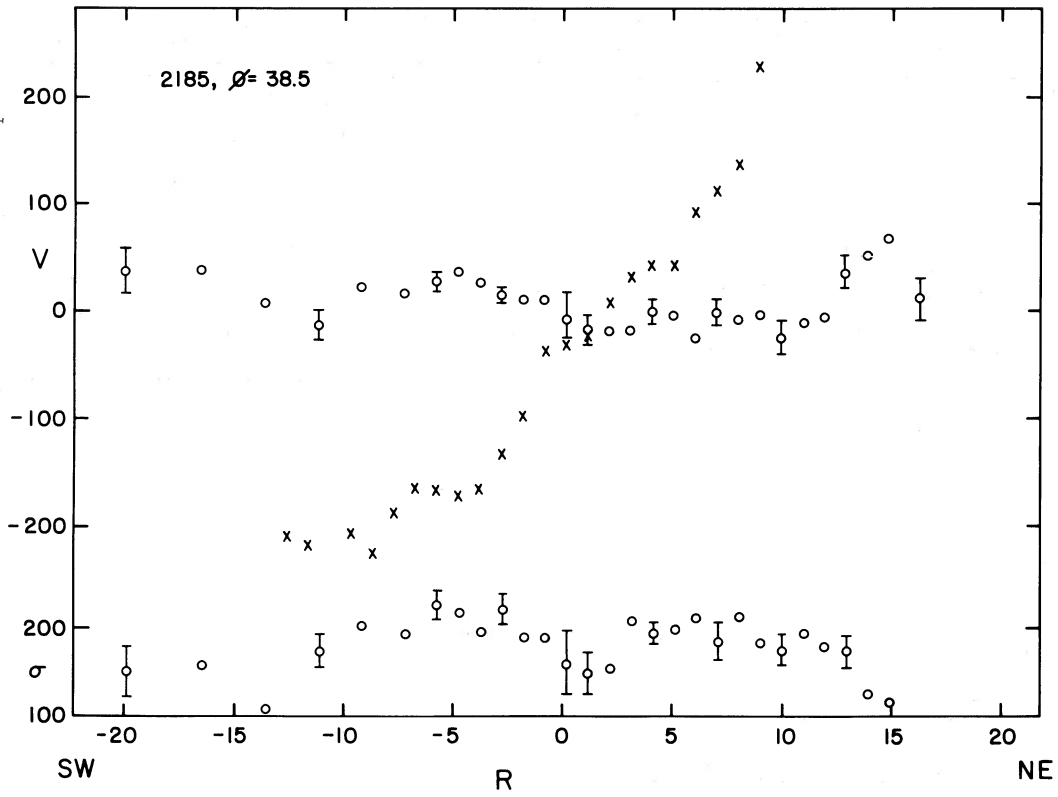


FIG. 4.—Rotation curve and velocity dispersion profile at P.A. = 38°.5. Symbols as in Fig. 2.

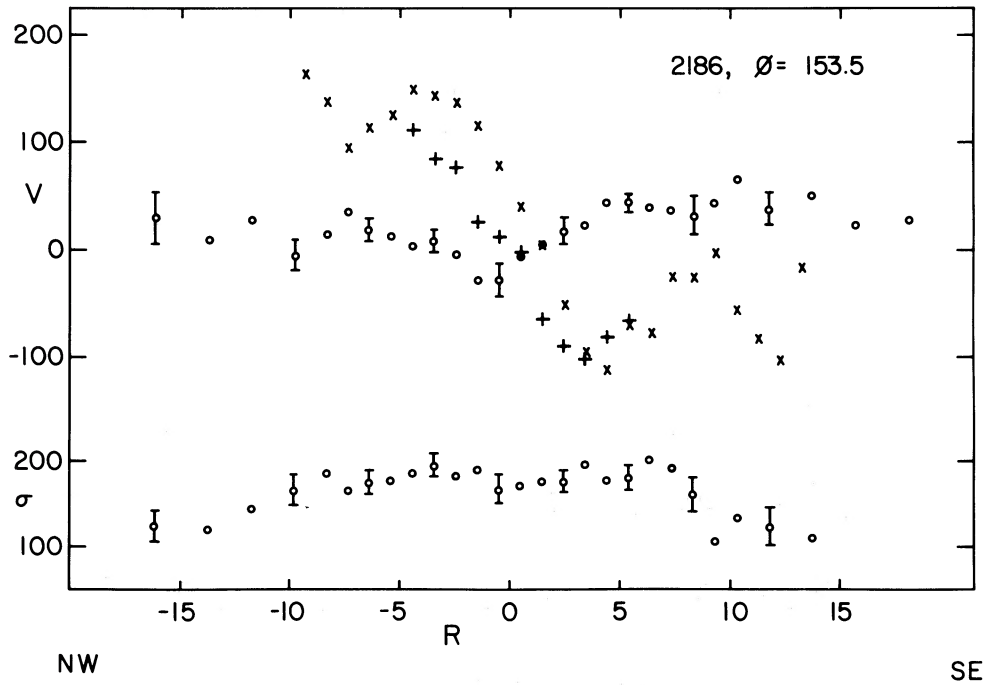


FIG. 5.—Rotation curve and velocity dispersion profile at P.A. = 153°.5. Symbols as in Fig. 2.

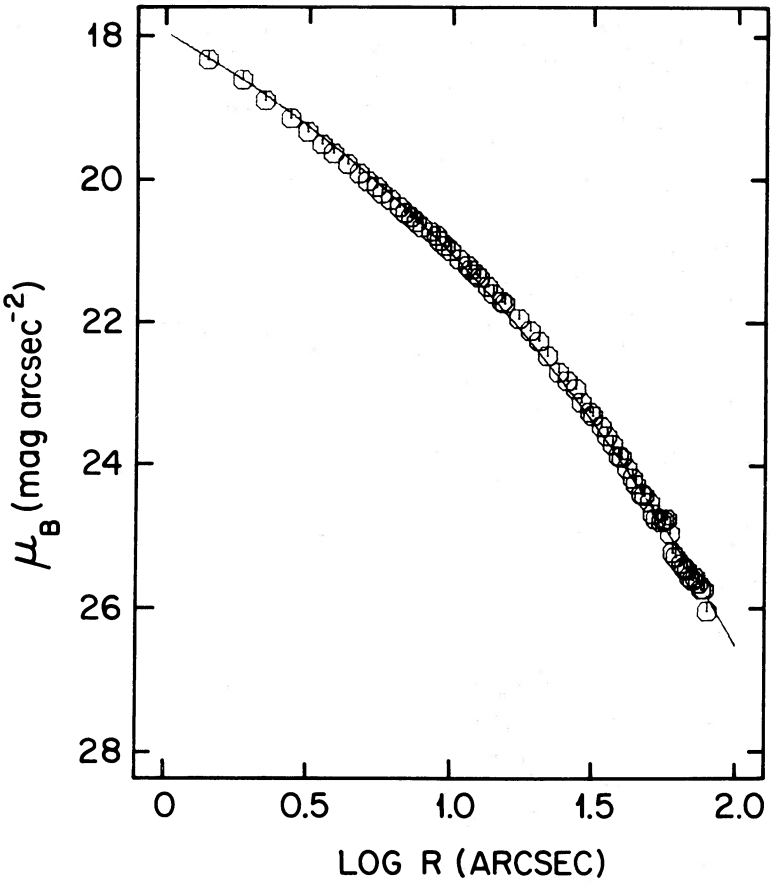


FIG. 6.—Surface brightness profile for NGC 7097. The solid line is a fit of a de Vaucouleurs law with effective radius 4.86 kpc.

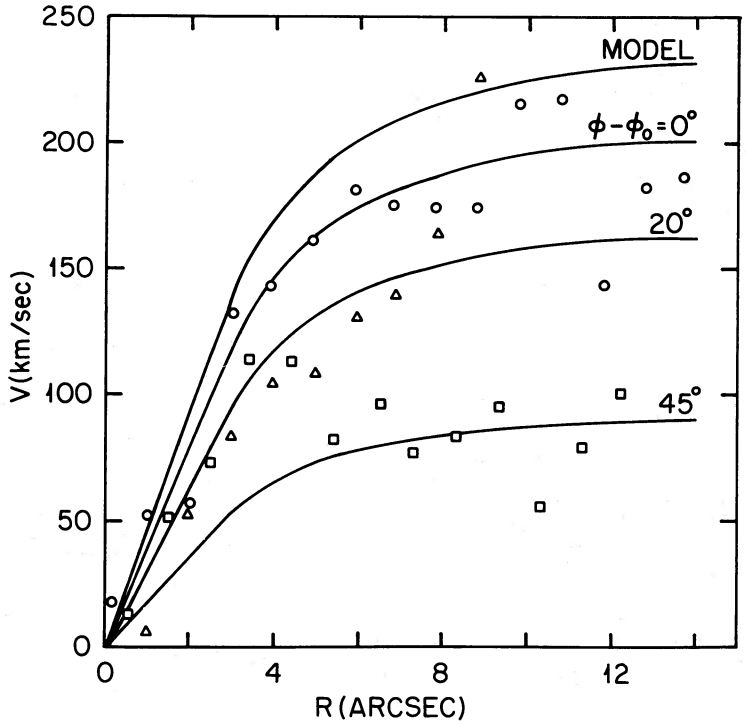


FIG. 7.—Rotation curves for the gas disk model compared to the observations at four position angles. "Model" shows the adopted rotation curve. Each additional line labels the predicted curve at each observed position angle. The points show the observations at $\phi - \phi_0 = 0°$ (*open circle*), 20° (*open triangle*), and 45° (*open square*).

for the rest of this discussion. Just as the extent gives the inclination, the observed gas rotation curves give the circular velocity at each point in the disk. At a position $x$, $y$ in the galaxy, the gas velocity of a tilted disk is

$$V_0(x, y) = V_c(r)(x/r) \sin i \, .$$

Note that $r$ is the distance from the center in the disk ($r^2 = x^2 + y^2 \sec^2 i$). For a disk with inclination near 60°, the appropriate approximation is to treat the major axis rotation curve as a measure of $V_0(x, 0) = V_c(r = x) \sin i$. So in this simple case, the circular velocity can be recovered from division by sin $i$. The result of this simple calculation as applied to a smoothed major axis rotation curve is shown in Figure 7 as the adopted model. Similarly, the velocity predicted by the inclined disk model can be compared to the observations at each position angle as shown in Figure 7.

Another approach is to fit equation (2) to the observed gas velocities by adopting a function shaped like the "model" curve in Figure 7 with an unknown inclination, major axis position angle, amplitude, and scale length. As a check on our empirical approach, we carried out this exercise. The goodness of fit was assessed by computing $\chi^2$, and the resulting four dimensional parameter space was surveyed. The minimum fit had an inclination of 50° and velocities larger by 15% than those of the "model" curve. This independent assessment of the inclination is in reasonable agreement with our estimate above and provides an estimate of the uncertainty in this quantity. The resulting increase in $M(r)$ makes no substantial difference in the dynamical results derived below. Indeed, although the uncertainty in the inclination is moderately large, the mass-to-light ratio derived is quite insensitive to the details of this fit.

Given the rotation curve, it is straightforward to infer the spherical mass distribution that would produce it, since

$$\rho(r) = (4\pi r^2 G)^{-1} d/dr(v_c^2 r) \, . \quad (3)$$

It is of interest to compare the mass distribution with the light distribution. The luminosity density required to produce the observed light distribution is shown in Figure 8, as computed from Young's (1976) tabulation for the de Vaucouleurs law. This figure makes it clear that the mass distribution required to produce the gas rotation is different from the light distribution required to match the stellar luminosity distribution. The mass-to-light ratio is below 1 at the center and rises to 3.5 at 3 kpc, as can be determined directly from the figure. This result does not depend on the use of a de Vaucouleurs law model, since we obtain the same result for luminosity density using the method described in Richstone and Tremaine (1984).

For comparison, we have calculated the mass-to-light ratio ($M/L$) via King's core-fitting method (Rood *et al.* 1972) using the central velocity dispersion of 200 km s$^{-1}$ and a core radius corresponding to 1″ which we take to be an upper limit. We find a value near 12. King's method has severe shortcomings if the velocity dispersion is anisotropic or if the core is unresolved (Richstone and Tremaine 1984; Schweizer 1979). However, it is widely used for estimating $M/L$ for elliptical galaxies. It is of interest that our detailed treatment gives a qualitatively different result.

It might be argued that the observed gas is not supported primarily by rotation, and that the mass distribution derived under that assumption is misleading. Three alternatives to rotational support are infall, outflow, and random motions of gas clouds. The first two pictures require rapid replenishment

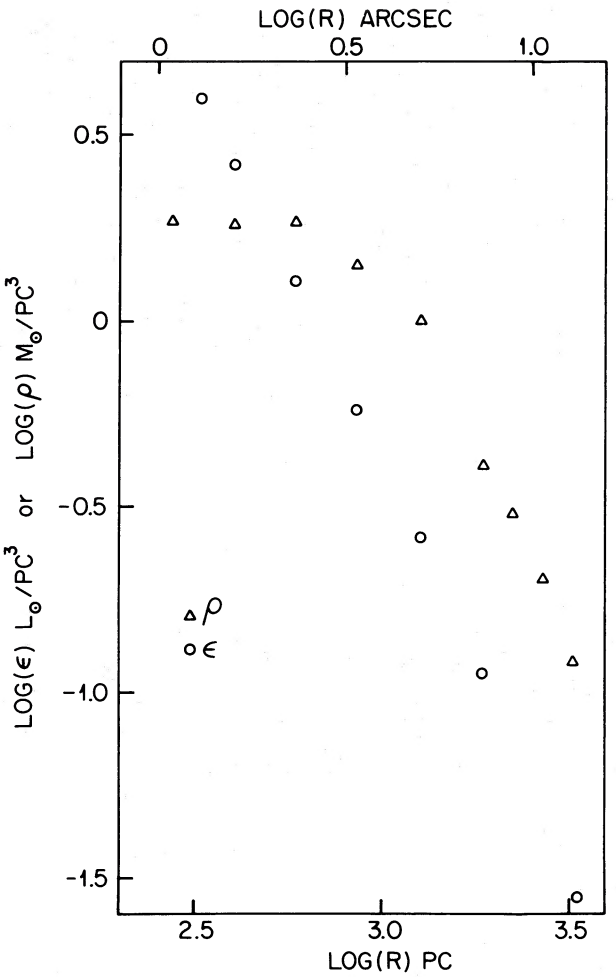


FIG. 8.—Derived mass density distribution (*open circle*) and luminosity density distribution (*open triangle*) for NGC 7097. The local mass-to-light ratio is just the ratio of these quantities, easily read from the logarithmic scale.

of gas from a reservoir (for infall) or an unseen source of angular momentum (for outflow). For random motions to play an important role, the velocities must approach the observed rotational velocities. For $r < 500$ pc, the velocities would be of order 50 km s$^{-1}$ and might escape detection. But for $r > 1$ kpc, random velocities of 150 km s$^{-1}$ would be required which would broaden the emission lines noticeably. Because no such broadening is observed, and because our kinematic model of a cold disk matches the observed velocities, we believe the derived mass distribution should be taken seriously.

## IV. INTERPRETING THE STELLAR DYNAMICAL DATA

On the major axis, the stellar rotational velocities reach a maximum of 30 km s$^{-1}$ corresponding to $v/\sigma < 0.15$. Hence, as is usually the case, the rotation of the galaxy is insufficient to account for its E4 figure. On the minor axis ($\phi = 108.5$), a velocity gradient may be present, but it corresponds to a rotation speed no larger than 30 km s$^{-1}$. Thus, the projection on the sky of the stellar population's angular momentum vector lies in the southeasterly direction.

Since the gas velocities are in the opposite direction from the stars, the projection on the sky of the gas angular momentum vector lies in a westerly or northwesterly direction. Although two nearly aligned vectors can be projected in substantially

different directions, the amplitude of the gas rotation curve implies that the gas angular momentum vector lies less than 30° from the plane of the sky. Thus, the angular momentum of the stars must be (at the very least) nearly orthogonal to, if not actually opposed to the gas.

This difference in angular momentum orientation indicates that this gas could not have been shed by the observed stellar population or any set of stars with dynamics resembling the observed population. Although this situation is reminiscent of a number of other cases where the gas angular momentum is orthogonal to the stellar angular momentum, the result in this case is not a bizarre or peculiar galaxy, but a very ordinary elliptical with a disk that has settled into the plane that includes the projected major axis. Shane (1980), Richstone and Potter (1982), and Schechter, Ulrich, and Boksenberg (1984) have argued that gas of this general type is either delayed infall or a wrecked companion. The presence of oxygen lines shows that the gas is not primordial and may give a hint of its origin.

The stellar velocity dispersion measurements out to 15″ on the major axis permit us to employ the linear programming method of Richstone and Tremaine (1984, 1985) to determine the mass-to-light ratio and velocity anisotropy of the galaxy. For that method, a mass distribution is assumed, and then a complete set of time-averaged orbits is constructed in that mass distribution. For each orbit, the contribution to the light distribution at each point and the projected velocity dispersion

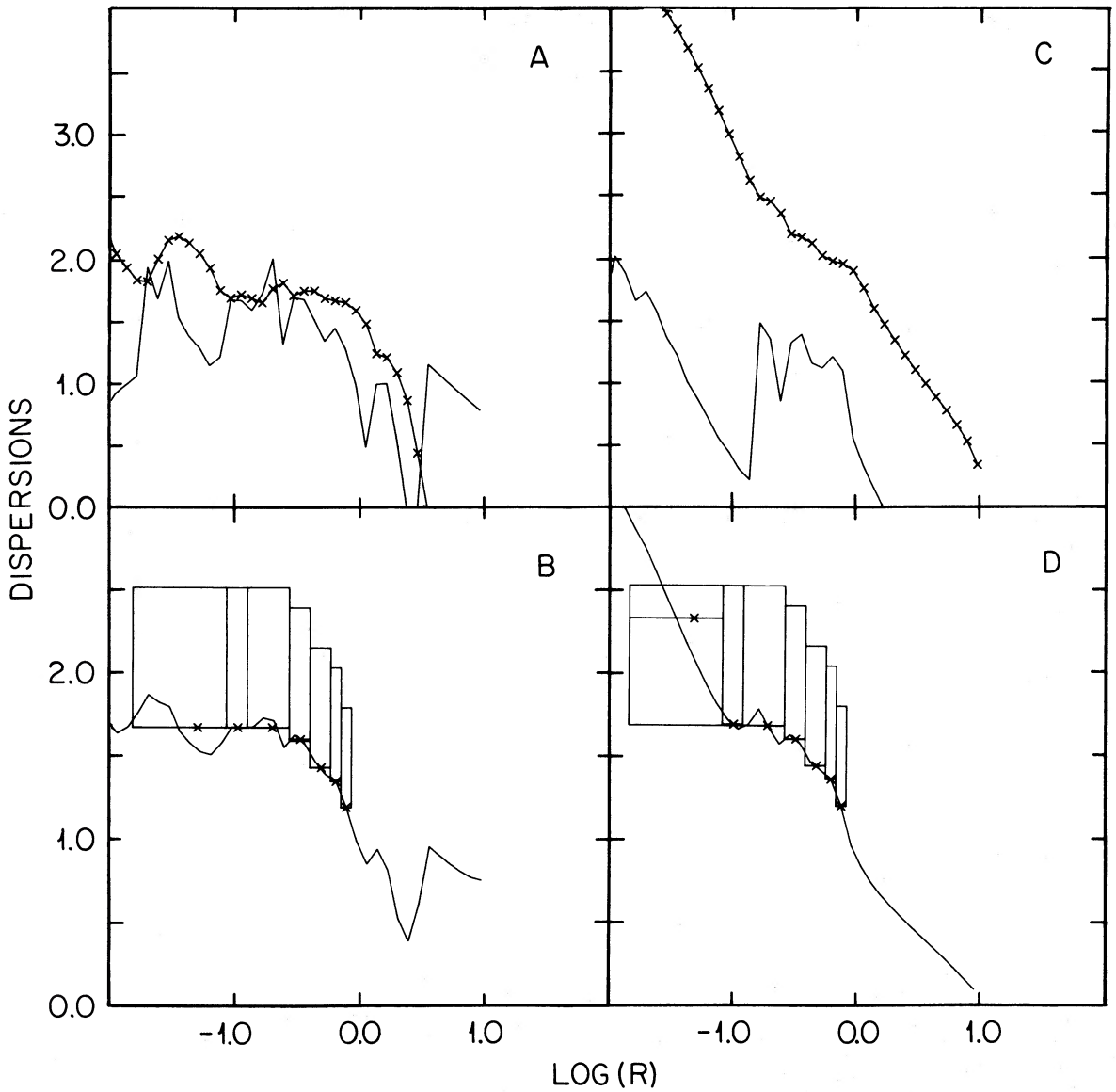


FIG. 9.—(*a*) Radial (*cross*) and tangential (*solid line*) velocity dispersion profiles for models with the *maximum* tangential velocity dispersion consistent with the light distribution of the galaxy, a constant $M/L$ of 3.5 (set from the gas velocities at 3 kpc), and the observed dispersions. The dispersions are in units of 100 km $s^{-1}$, and $R$ is in units of the effective radius (4.86 kpc). (*b*) Projected stellar velocity dispersion profile which would be observed for the model detailed in (*a*). The contiguous rectangles bound the range of velocity dispersions consistent with the observations over each range in radius. The symbols (*crosses*) show the model's light-averaged velocity dispersion within the radius range covered by the box. Since this solution has the maximum allowable tangential velocity dispersion, but has a smaller tangential dispersion than radial dispersion, no isotropic model can satisfy the constraints. (*c*) As in (*a*), but now with the *minimum* allowable tangential velocity dispersion. (*d*) As in (*b*), but now using the velocity dispersions shown in (*c*).

are tabulated. Using a linear programming code, weighted sums of the orbits can be found which match the galaxy light distribution at all points and which also match (within the errors) the observed velocity dispersions. This technique permits us to find the maximum and minimum $M/L$ and velocity anisotropy that can match the data. We have concentrated on matching the data with sets of orbits that probe the extremes of velocity anisotropy.

We constructed three sets of dynamical models for NGC 7097 under different assumptions about its mass distribution. In each case, we treated the galaxy as though it were spherically symmetric. We discuss the dangers of this idealization after presenting the results.

Our first assumption (case A) concerning the mass distribution was that the galaxy's unknown $M/L$ is independent of radius. This case amounts to ignoring all the information derived from the gas velocities. In this case, the galaxy $M/L$ is in the range 3 to 7, and the velocity anisotropy can favor either predominantly radial or predominantly tangential orbits. However, the models where tangential orbits dominate do not reproduce the drop in $\sigma$ seen in Figure 2.

In case B, we assume that $M/L$ is constant, but that the gas is in circular orbits at large radii (15″). This sets the galaxy $M/L$ at 3.5. In this case, all models that fit the data favor radial velocity dispersions over tangential dispersions. Figure 9 shows the minimum and maximum tangential velocity disper-

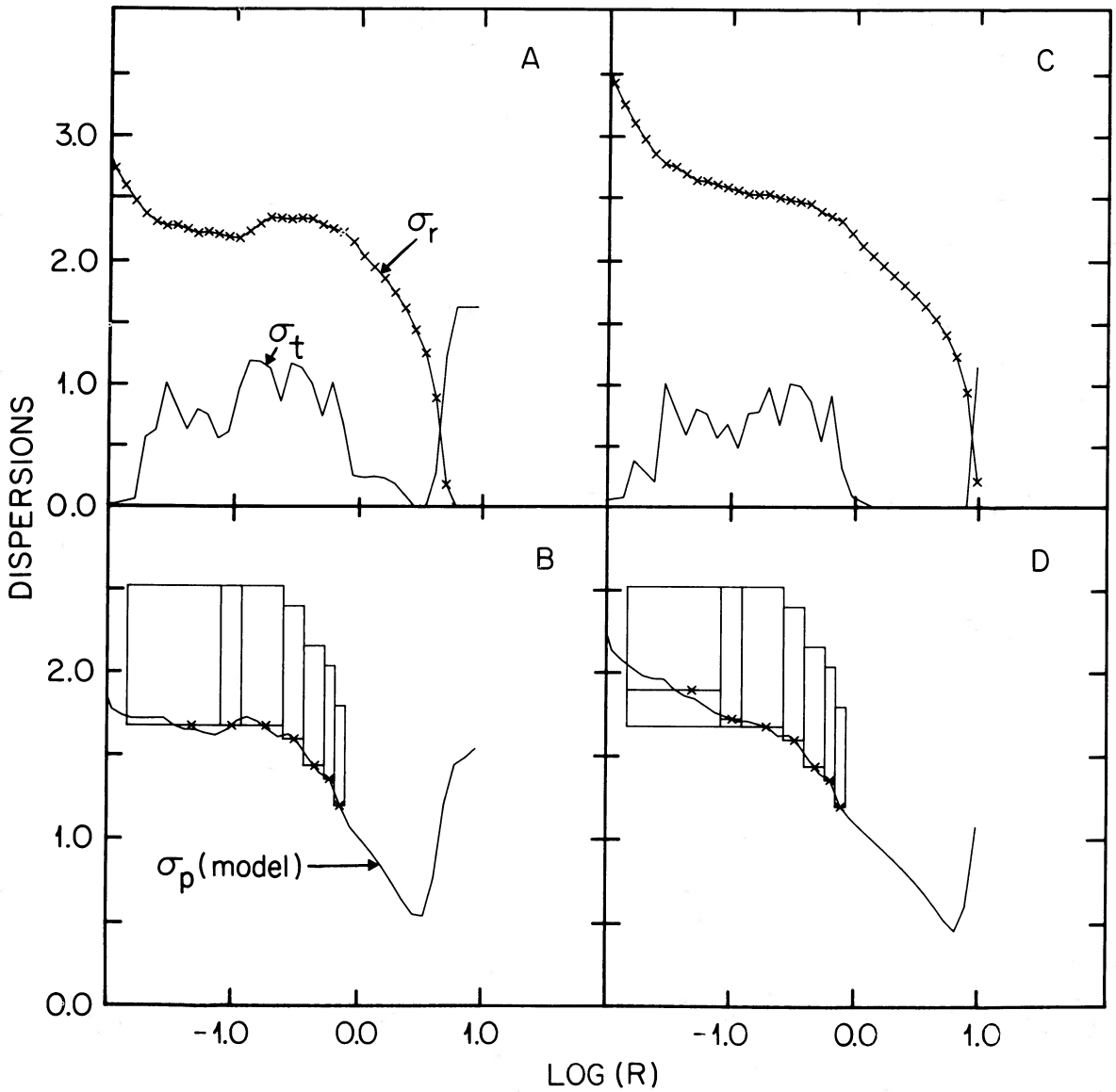


FIG. 10.—Same as Fig. 9, but now for variable $M/L$ models with mass distributions derived from the gas velocities, assuming they are circular, and the light distribution derived from the surface photometry. (*a*) Radial (*cross*) and tangential (*solid line*) velocity dispersions for the model with the maximum allowed tangential dispersion. (*b*) Projected velocity dispersion compared to the observations for the velocity dispersions shown in (*a*). As in Fig. 9, the rectangles show the range of velocity dispersion allowed by the observations in a range of radius. (*c*) Radial (*cross*) and tangential (*solid line*) velocity dispersions for the same model with the minimum allowed tangential dispersion. (*d*) Projected velocity dispersion compared to the observations for the velocity dispersions shown in (*c*). Under these assumptions, all the models, even those with the maximum allowable tangential velocity dispersion, are dominated by very elongated orbits.

sion models for this case. Even with the maximum allowable tangential component, the galaxy model is dominated by radial orbits.

For case C, we take seriously the mass distribution derived from the model of a gas disk given in § III, and shown in Figure 8. Including the effect of varying $M/L$ with position as illustrated in Figure 8 yields the minimum and maximum tangential component models shown in Figure 10. The models are nearly identical, and each has much more energy in radial motion than is allowed in tangential motion.

Relaxing the constraint of spherical symmetry is unlikely to change the character of the results. An E4 mass distribution would require 50% less mass for the rotation curve, but changing $M/L$ by 50% would not change qualitative features of the case B results: radial orbits would still be favored. A flattened model might make the case C solutions even more extreme, although they already are very stringent.

To summarize: it seems very likely that this galaxy has a stellar velocity distribution which is dominated by radial orbits. This conclusion can be avoided only if the gas observed in emission lines is nowhere in circular orbits and if the stellar velocity dispersion measurements are systematically high in the center or low at radii beyond 10″.

## V. DISCUSSION

NGC 7097 provides an unusually favorable case for probing the dynamics of an elliptical galaxy. We have observed the rotation of a gas disk and the motions of the stars to build a picture for the galaxy which is more tightly constrained than in most investigations of ellipticals.

The gas may well be present because of cannibalism of a gas rich object. In any event, the large difference between the gas motion and the stellar motion appears to rule out gas with the same origin as the stars.

The mass model derived from the gas disk requires a different mass distribution than the light distribution derived from the photometric profile of the galaxy. The corresponding change in $M/L$ is large and is not accompanied by any hint of change in the stellar component of the galaxy. If this galaxy has no significant color gradient or change in line strength that might hint at variations in the stellar population, then the possibility of a dark halo similar to those inferred for spiral galaxies becomes an attractive idea. Evidence for dark matter in ellipticals has been elusive: this may be a good way to find it.

Once the mass distribution is established from the disk's rotation curve, the linear programming approach to understanding the stellar orbits becomes especially illuminating. In this case, the distribution function that matches the observations is dominated by very elongated orbits.

Taken at face value, the two key results of this paper offer important and provocative tests for models of galaxy formation. The estimate of $M/L$ below 1 at the center of this galaxy conflicts with a value of 12 found from the conventional core fitting method. This may imply that the usual values quoted for ellipticals are substantially in error. In this case, the error arises because the galaxy core is unresolved and the velocity dispersions are anisotropic. For most elliptical galaxies, the central $M/L$ is derived with less information, and it is possible both that there is a substantial range in the real $M/L$ and that the conventional numbers are biased. In any event, the evidence for a distribution function with many elongated orbits provides a challenge for galaxy formation theories. We would suppose that spherical or ellipsoidal collapse from a cold Hubble flow would more easily populate nearly radial orbits (Gott 1977) than mergers would (as, for example, in the very detailed calculations of Farouki, Shapiro, and Duncan 1983). Moving from supposition to confidence in that proposition will require further theoretical work which could be nearly as useful in clarifying this issue as improved observations of this galaxy and those like it.

Research on the dynamics of galaxies at the University of Michigan is supported in part by NSF grant AST 83-11414.

## REFERENCES

Bertola, F., Bettoni, D., Rusconi, L., and Sedman, G. 1984, *A.J.*, **285**, 527.
Caldwell, N. 1984, *Pub. A.S.P.*, **96**, 287.
Demoulin-Ulrich, M.-H., Butcher, H. R., and Boksenberg, A. 1984, *Ap. J.*, **285**, 527.
Farouki, R. T., Shapiro, S. L., and Duncan, M. J. 1983, *Ap. J.*, **265**, 567.
Gott, J. R. 1977, *Ann. Rev. Astr. Ap.*, **15**, 233.
Richstone, D. O., and Potter, M. 1982, *Nature*, **298**, 728.
Richstone, D. O., and Tremaine, S. 1984, *Ap. J.*, **286**, 27.
———. 1985, *Ap. J.*, **296**, 370.
Rood, H. J., Page, T. L., Kintner, E. C., and King, I. R. 1972, *Ap. J.*, **179**, 627.
Sandage, A. R., and Visvanathan, N. 1978, *Ap. J.*, **225**, 742.
Sargent, W. L. W., Schechter, P. L., Boksenberg, A., and Shortridge, K. 1977, *Ap. J.*, **212**, 326.
Schechter, P. L., Ulrich, M. H., and Boksenberg, A. 1984, *Ap. J.*, **277**, 5226.
Schweizer, F. 1979, *Ap. J.*, **233**, 23.
Shane, W. W. 1980, *Astr. Ap.*, **82**, 314.
Young, P. J. 1976, *A.J.*, **81**, 807.

NELSON CALDWELL: Cerro Tololo Inter-American Observatory, Casilla 603, La Serena, Chile

ROBERT P. KIRSHNER: Harvard-Smithsonian Center for Astrophysics, 60 Garden St., Cambridge, MA 02138

DOUGLAS O. RICHSTONE: Department of Astronomy, University of Michigan, Ann Arbor, MI 48109-1090